carboxylate hydrogen bonding make the largest contribution, and the contrasting VCD spectra in the methine stretching region, where conformations with gauche NH···CO and CO···HC_β rings are required for enhancement of the VCD intensity.

The pH dependence of the methine bending VCD spectra does not always parallel that of the methine stretches. These results can also be understood within the ring current framework. In L-alanine at low pH, protonation of the carboxylate group eliminates the interaction with the β-hydrogen, and the conformation with carboxyl to trans NH hydrogen bonding predominates, removing the source of the intensity enhancement of the methine stretch. The NH···OC interaction may also be weaker with a neutral carboxyl group. In the bending region at low pH, the symmetric carboxyl stretch (primarily single-bond stretch) occurs at 1262 cm^{-1}, and two distinct methine bending modes are no longer observed. Both the weakening of the hydrogen bond and the alteration of the nature of the normal modes serve to decrease the methine bending VCD intensity. Similarly, at high pH, isolated methine bending bands are not observed, possibly because of mixing with NH_2 motions, but a localized methine stretching mode and the β-hydrogen interaction are maintained. Thus enhanced methine stretching VCD, but not bending VCD, is observed at high pH.

In Gly-L-Ala, enhanced methine stretching VCD is observed at both low and high pH. To account for the low pH results, we postulated a conformation with a seven-membered ring closed by hydrogen bonding between the peptide C=O and carboxyl OH groups.[9] The methine stretch can generate current around this ring, enhancing the VCD intensity. However, compared to the conformation at neutral pH, the molecular environment for the methine bends is quite altered. Isolated methine bending modes are no longer observed, and no VCD intensity is generated. Since high pH alters the glycyl residue, but not the L-alanyl residue, enhanced VCD for both the methine stretch and bends is observed for Gly-L-Ala at high pH.

Finally, we note that Diem has recently carried out a study of the midinfrared VCD spectra of L-alanine in H_2O and D_2O, using a dispersive VCD instrument, that includes the 1600- and 1250–900-cm^{-1} regions.[29] In the frequency region (1250–1500 cm^{-1}) that our studies overlap, the VCD spectra are nearly identical in pattern.

Conclusions

The methine bending VCD spectra of L-amino acids and dipeptides can provide information on absolute configuration and local intramolecular association. The occurrence of the characteristic (−,+) VCD pattern depends on several factors: (1) the presence of two isolated, approximately orthogonal methine bending modes directed primarily toward the carboxylate and amino groups; (2) the presence of a CO_2^- group adjacent to the methine bond; (3) the presence of a ring closed by hydrogen bonding between a carboxylate oxygen and the peptide NH bond or the NH bond trans to the methine. Since the methine bends occur in the midinfrared region with numerous other types of deformation and stretching motion, in many environments the methine bends may mix extensively with other motions. In such a delocalized mode, the methine bends may not be directed toward the amino or carboxylate group, and thus may not generate any ring current. Alternatively, the net electric dipole transition moment for the mixed mode may not overlap favorably with any ring current magnetic moment generated by methine motion. For these reasons enhanced methine bending VCD may not be observed even in cases for which the methine stretch exhibits strong ring-current enhanced VCD intensity. However, since the methine bends, but not the methine stretches, can be observed in H_2O solution, VCD spectra in both vibrational regions provide valuable conformational and configurational probes for amino acids and dipeptides.

Acknowledgment. This work was supported by grants from the National Institutes of Health (GM-23567) and National Science Foundation (CHE 86-02854).

Registry No. Gly-L-Ala, 3695-73-6; L-Ala-Gly, 687-69-4; L-Ala-L-Ala, 1948-31-8; L-Ala, 56-41-7; L-Pro, 147-85-3; (*s*)-glycine-*C*-d_1, 62061-52-3.

(29) Diem, M. *J. Am. Chem. Soc.*, preceding paper in this issue.

Principal Component–Three Component Self-Modeling Analysis Applied to *trans*-1,2-Di(2-naphthyl)ethene Fluorescence[1]

Ya-Ping Sun,[†] Donald F. Sears, Jr.,[†] Jack Saltiel,*[,†] Frank B. Mallory,[‡] Clelia W. Mallory,[§] and Carolyn A. Buser[‡]

Contribution from the Departments of Chemistry, The Florida State University, Tallahassee, Florida 32306, Bryn Mawr College, Bryn Mawr, Pennsylvania 19010, and University of Pennsylvania, Philadelphia, Pennsylvania 19104. *Received April 4, 1988*

Abstract: Fluorescence spectra of *trans*-1,2-di(2-naphthyl)ethene, DNE, obtained under varying conditions of excitation wavelength and oxygen and carbon tetrachloride concentrations in methylcyclohexane were resolved into three distinct components by application of principal component analysis combined with a three-component self-modeling technique. Spectral matrices for O_2 and CCl_4 quenching, treated separately, yielded nearly identical pure component fluorescence spectra. The spectra were assigned to each of the three conformers of DNE by comparison with spectra of 3-methyl derivatives. Stern–Volmer quenching plots for the individual conformers were shown to be independent of excitation wavelength, indicating that each conformer has a single lifetime.

Upon excitation, flexible molecules containing conjugated double bonds undergo reversal of single/double bond order. Conformational changes which occur freely in the ground state are often too slow in singlet and triplet lowest excited states leading to noninterconverting excited molecules with different structures and properties. Since each ground-state equilibrium conformation has its own distinctive absorption spectrum, different excitation wavelengths, λ_{exc}, can lead to different compositions of excited

[†] The Florida State University.
[‡] Bryn Mawr College.
[§] University of Pennsylvania.

(1) Presented in part at the 39th Southeast Regional American Chemical Society Meeting, November 1987, Orlando, FL; Abstr. no. 151.

0002-7863/88/1510-6974$01.50/0

conformers and consequently to changes in photochemical behavior. Control of the photochemistry of such molecules by preferential excitation of different ground-state conformations was first recognized by Havinga for trienes related to vitamin D.[2] The principle of nonequilibrating excited rotamers (NEER) was Havinga's generalization of this concept.[2] An early example of this principle was the triplet-sensitized dimerization of 1,3-dienes which was explained by Hammond and co-workers by postulating selectively excited nonequilibrating s-cis and s-trans diene triplet intermediates.[3] It was later demonstrated that *s-cis* and *s-trans*-1,3-diene triplets have different cis–trans decay ratios and that their selective formation plays an important role in sensitized cis–trans photoisomerization.[4] Since dienes and trienes are generally nonfluorescent and their transient absorptions are not well characterized, such mechanistic conclusions rest on indirect measurements, namely the dependence of photochemical response either on λ_{exc} or on the triplet energy of the donor.

The complementarity of fluorescence and photoisomerization played an important role in the elucidation of the mechanism for cis–trans photoisomerization of the stilbenes.[5] We were therefore intrigued by reports of λ_{exc} dependent fluorescence spectra and biexponential fluorescence decay in 1,2-diarylethenes.[6] The goal of quantitatively associating photophysical and photochemical behavior with individual conformers seemed tenable in such systems. The fluorescence of *trans*-1-phenyl-2-(2-naphthyl)ethene, NPE, had been thoroughly studied and appeared to arise from superposition of the emissions from two nonequilibrating excited conformers having ≃5 and ≃25 ns lifetimes at room temperature.[7]

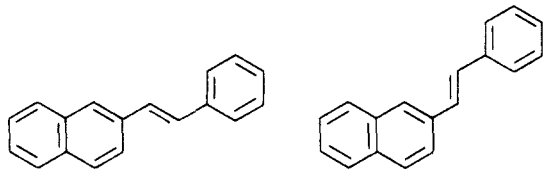

Fischer's group assigned pure fluorescence spectra for each conformer based on observations at 77 K,[7a] while Birks and co-workers calculated pure conformer fluorescence excitation and emission spectra by using an elegant analysis of the λ_{exc} and λ_{em} dependence of fluorescence decay curves.[7b] The challenge of obtaining pure component fluorescence spectra directly by analysis of mixtures of NPE_1 and NPE_2 fluorescence spectra prompted our first application of the combination of principal component analysis with the self-modeling technique, PCA-SM,[8] first proposed by Lawton and Sylvestre.[9] Molecular structures were assigned to the spectra obtained for the two conformers by comparison with spectra for conformationally restricted analogues.[8,10]

trans-1,2-Di(2-naphthyl)ethene, DNE, appeared to be an excellent candidate for the extension of the PCA-SM approach to a three-component system. Contributions from a minimum of two components in fluorescence were indicated by biexponential decay[7a] and by time-resolved fluorescence spectra.[13] The presence of three components was observed in fluid solution at room temperature by selective excitation of fluorescence with different λ_{exc},[6d] and spectra of this type were given for DNE selectively excited in a polyethylene film at −100 °C.[6b] The latter medium was thought to allow the freezing in of an equilibrium conformer composition corresponding to a higher temperature and thus to larger contributions from the higher energy conformers B and C.[6b] Nonequilibrium conformer mixtures of *trans*-DNE containing even larger contributions from C were also achieved by UV irradiation of *cis*-DNE in frozen ethanol or decalin at −175 and −145 °C, respectively.[14] In addition, the presence of two components (B, C) in DNE fluorescence, obtained by exciting the long wavelength onset of DNE absorption, had been inferred from the differential quenching of this fluorescence by CCl_4.[13b]

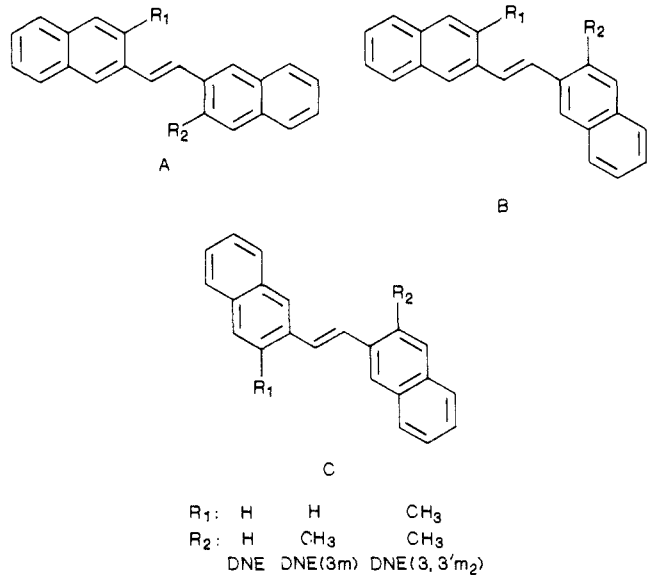

We have published a preliminary report of a PCA-SM treatment of DNE fluorescence spectra obtained at different λ_{exc} and oxygen concentrations which relied on fluorescence spectra of 3-methyl, DNE(3m), and 3,3'-dimethyl, DNE(3,3'm_2), derivatives in defining two of the three pure component spectra of DNE.[15] It was assumed that, for steric reasons, replacement of the hydrogen at R_2 restricts the system to only conformers B and C and that a second methyl group at R_1 further restricts the system to conformer C. We have since developed a PCA-SM method which allows analysis of DNE fluorescence spectra directly without the aid of the methyl derivative spectra.[16] This paper reports the results of the application of this method to two sets of DNE fluorescence spectra and evaluates the success of our previous methyl derivative approach.

Results

Mathematical Procedure. Sets of fluorescence spectra obtained for each olefin solute by varying λ_{exc} and $[O_2]$ or $[CCl_4]$ were used to create separate input matrices for application of PCA-SM. On the basis of the eigenvalues and eigenvectors derived, each matrix behaved cleanly as a two- or three-component system, except for DNE(3,3'm_2) whose spectra are independent of changes in experimental conditions and exhibited a single component. Accordingly, with the exception of DNE(3,3'm_2), normalized ex-

(2) For a review, see: Jacobs, H. J. C.; Havinga, E. *Adv. Photochem.* **1979**, *11*, 305.
(3) Liu, R. S.; Turro, N. J.; Hammond, G. S. *J. Am. Chem. Soc.* **1965**, *87*, 3406.
(4) Saltiel, J.; Metts, L.; Sykes, A.; Wrighton, M. *J. Am. Chem. Soc.* **1971**, *93*, 5302.
(5) For reviews, see: (a) Saltiel, J.; D'Agostino, J. T.; Megarity, E. D.; Metts, L.; Neuberger, K. R.; Wrighton, M.; Zafiriou, O. C. *Org. Photochem.* **1973**, *3*, 1. (b) Saltiel, J.; Charlton, J. L. *Rearrangements in Ground and Excited States*; de Mayo, P., Ed.; Academic Press: New York, 1980; Vol. 3, p 25.
(6) For reviews, see: (a) Scheck, Y. B.; Kovalenko, N. P.; Alfimov, M. V. *J. Lumin.* **1977**, *15*, 157. (b) Fischer, E. *J. Photochem.* **1981**, *17*, 331. (c) Mazzucato, U. *Pure Appl. Chem.* **1982**, *54*, 1705. (d) Fischer, G.; Fischer, E. *J. Phys. Chem.* **1981**, *85*, 2611.
(7) For key references, see: (a) Haas, E.; Fischer, G.; Fischer, E. *J. Phys. Chem.* **1978**, *82*, 1638. (b) Birks, J. B.; Bartocci, G.; Aloisi, G. G.; Dellonte, S.; Barigelletti, F. *Chem. Phys.* **1980**, *51*, 113.
(8) Saltiel, J.; Eaker, D. W. *J. Am. Chem. Soc.* **1984**, *106*, 7624.
(9) Lawton, W. H.; Sylvestre, E. A. *Technometrics* **1971**, *13*, 617.
(10) Our preliminary PCA-SM generated conformer spectra were based on a rather small spectral input matrix and though in agreement with Fischer's low *T* spectra are at variance with spectra obtained by Bartocci, Mazzucato, and co-workers[11] through a more refined treatment of decay curves with Birks' approach.[7b] PCA-SM treatment of larger spectral input matrices has confirmed this latter solution.[12]
(11) Bartocci, G.; Mazzucato, U.; Masetti, F.; Aloisi, G. G. *Chem. Phys.* **1986**, *101*, 461.
(12) Saltiel, J.; Sears, D. F., Jr.; Choi, J.-O.; Mallory, F. B.; Mallory, C. W., unpublished results.
(13) (a) Ghiggino, K. P. *J. Photochem.* **1980**, *12*, 173. (b) Matthews, A. C.; Sakurovs, R.; Ghiggino, K. P. *J. Photochem.* **1982**, *19*, 235.
(14) Castel, N.; Fischer, E. *J. Mol. Struct.* **1985**, *127*, 159.
(15) Saltiel, J.; Sears, D. F., Jr.; Mallory, F. B.; Mallory, C. W.; Buser, C. A. *J. Am. Chem. Soc.* **1986**, *108*, 1688.
(16) Sun, Y.-P.; Sears, D. F., Jr.; Saltiel, J. *Anal. Chem.* **1987**, *59*, 2515.

perimental spectra, S_i, can be represented as linear combinations of two or three eigenvectors

$$\bar{S}_i = \alpha_i \bar{V}_\alpha + \beta_i \bar{V}_\beta + \gamma_i \bar{V}_\gamma \quad (1)$$

where the $\bar{V}$'s are the eigenvectors and $\alpha_i,\beta_i,\gamma_i$ is the ith set of combination coefficients. For the three-component systems the three eigenvectors define a normalization plane in α, β, and γ space

$$\alpha(\sum_{j=1}^{n} V_{\alpha j}) + \beta(\sum_{j=1}^{n} V_{\beta j}) + \gamma(\sum_{j=1}^{n} V_{\gamma j}) = 1 \quad (2)$$

where $V_{\alpha j}$, $V_{\beta j}$, and $V_{\gamma j}$ are jth elements of V_α, V_β, and V_γ, respectively, and on which all combination coefficients must fall. By analogy to three-component phase diagrams, all (α_i, β_i, γ_i) points representing S_i's are confined within a triangle in the normalization plane. The corners of the triangle correspond to the coefficients of the three pure-component spectra, designated here as A, B, and C and its sides correspond to the three combinations of two-component mixtures. The experimental spectra are also given by

$$S_i = x_{ia}A + x_{ib}B + x_{ic}C \quad (3)$$

where the x_i's are fractional contributions of each pure-component spectrum so that x_{ia}, x_{ib}, and x_{ic} must all be ≥ 0 and $x_{ia} + x_{ib} + x_{ic} = 1$. For a two-component system $\gamma = 0$, $\bar{V}_\gamma$ does not contribute in eq 1, eq 2 defines a normalization line in the α,β plane, and $x_{ic} = 0$ in eq 3.

As has been described in detail, success of our method for selecting pure-component coefficients for two- and three-component systems requires the existence of at least two wavelength regions, W_1, and W_2, in the fluorescence spectra where each of two components contributes uniquely. In the spectral sets treated in this paper such regions exist at the onset and tail parts of the spectra. It follows that by monitoring separately the onset and tail halves of resultant spectra, eq 1, for zero or very small negative intensities two sides of the triangle in α, β, γ space and the end points of the line in the α,β plane can be generated for three- and two-component systems, respectively. Finally, by requiring several points in each of the two critical regions to reach the base line simultaneously the possibility that experimental noise in the spectra will generate false limiting pure component coefficients is minimized. The selection of the limiting coefficients can be fine-tuned by application of any additional mathematical constraints which are dictated by the chemical and photophysical behavior of each system (see below).

Once pure component coefficients are selected, fractional contributions for each component, eq 3, can be calculated for three-component systems from

$$\begin{bmatrix} \alpha_i \\ \beta_i \\ \gamma_i \end{bmatrix} = \begin{bmatrix} \alpha_a & \alpha_b & \alpha_c \\ \beta_a & \beta_b & \beta_c \\ \gamma_a & \gamma_b & \gamma_c \end{bmatrix} \times \begin{bmatrix} x_{ia} \\ x_{ib} \\ x_{ic} \end{bmatrix} \quad (4)$$

where (α_a, β_a, δ_a) is the set of combination coefficients for spectrum A, and x_{ia} is the fractional contribution of component A in the ith experimental spectrum. Products of the fractional contributions times the area of each spectrum are proportional to the fluorescence quantum yields of the individual components for the corresponding experimental conditions.[8] It follows that when quencher concentration, [Q], is the experimental variable, the Stern–Volmer equation for each separate pure component is given by

$$\frac{x_j^0 A^0}{x_j A} = 1 + (K_{sv})_j[Q] \quad (5)$$

where A and A^0 are areas of the fluorescence spectra in the presence and in the absence of quencher, respectively (given by the corresponding normalization factors which were employed in constructing the input spectral matrix[8]), x_j and x_j^0 are fractional contributions of the jth component ($j = a$, b, or c, for a three-component system) with and without added quencher, and $(K_{sv})_j = k_{qj}\tau_j^0$ is the Stern–Volmer constant of the jth component (k_{qj} being the quenching rate constant and τ_j^0 the excited singlet lifetime in the absence of quencher of the jth component).

Evaluation of the adherence of points corresponding to combination coefficients for three-component experimental spectra to the derived triangle in the normalization plane can be achieved visually by giving the position of the points relative to orthogonal and edge views of the triangle. This task was accomplished by cartesian coordinate transformation of 0-α,β,γ into 0′-$\alpha'\beta'\gamma'$ where the γ' axis is orthogonal to the normalization plane, the β' axis is along the side of the triangle corresponding to the first and third components, and the new origin, 0′, is the corner of the triangle that corresponds to the third component.

DNE Fluorescence Spectra at λ_{exc} = 366 nm, [CCl_4]; 367 nm, [O_2]. Excitation near the onset of DNE's absorption spectrum, at 366 nm, gives a combination of DNE-B and DNE-C fluorescence in addition to scattered Rayleigh light centered at the excitation wavelength. Since DNE-B and DNE-C fluorescences are differentially quenched by CCl_4 in methylcyclohexane, MCH,[13b,16] use of a series of CCl_4 concentrations gives a three-component spectral input matrix. Resolution of this matrix served as the first application of our three-component PCA-SM method and has already been described.[16] In addition to giving the pure fluorescence spectra of DNE-B and DNE-C, the eigenvectors obtained and combination coefficients along the BC line of the triangle allow the accurate subtraction of the scattered light from the experimental spectra for later use.

Substitution of O_2 for CCl_4 as the quencher and PCA treatment of the resulting spectral matrix gave eigenvalues whose relative magnitude suggested the presence of only two components. Since scattered light at 367 nm was one of the two, the other had to be a combination of DNE-B and DNE-C. Oxygen's failure to cause a significant shift in the DNE-B/DNE-C fluorescence ratio will be traced below to similar Stern–Volmer constants and singlet lifetimes for the two conformers. Resolution into three components was achieved by treating a matrix consisting of triplicate emission spectra for each of three O_2 concentrations, one scattered light background spectrum centered at 367 nm, and the DNE-B fluorescence spectrum obtained from the CCl_4 data matrix (Figure 1-S). Application of our PCA-SM method[16] gave very closely spaced lines for 1 to 3 negligibly small negative intensities at the tail region of predicted spectra, eq 1, as potential triangle sides SB, and for three to nine such intensities at the onset region of predicted spectra as potential triangle sides SC. Lines centered in each region of potential sides were chosen as actual triangle sides. Coefficients for spectra B and C were selected by stepping along each two-component side until the predicted spectra were visually free of scattered light contributions. The triangle corner B thus obtained is very close to the point for the pure-component DNE-B fluorescence spectrum that had been included in the input matrix. The scattered light was subtracted from each experimental spectrum by using calculated fractional contributions of the three pure-component spectra (Figure 2-S), based on the final SBC triangle (Figure 3-S).

DNE Fluorescence Spectra at Several λ_{exc}, [CCl_4]. A set of DNE spectra in MCH was obtained by using five CCl_4 concentrations in 0.2 M increments from 0 to 0.8 M and exciting at 318, 329, 343, 355, and 366 nm. Five spectra were recorded for each λ_{exc}, [CCl_4] combination resulting in a total of 125 spectra. The 366-nm spectra were freed from scattered light prior to inclusion in the spectral matrix using the PCA-SM treatment described above.[16] Each row of the matrix consisted of the relative emission intensities of a spectrum at each of 150 wavelengths in the 340–489 nm range. Normalization was achieved by requiring the sum of the emission intensities for each spectrum to equal unity. Also included in the matrix were the pure DNE-B and DNE-C spectra obtained independently from the 366-nm data. Application of PCA to the resulting 127 × 150 data matrix gave eigenvalues and corresponding eigenvectors (Figure 1), consistent with a three-component system. Results from the search for the triangle in the normalization plane of the eigenvectors are shown in Figure 2 as projections on the α,β plane. The AB and BC sides of the triangle were sought by monitoring the tail half and the onset half

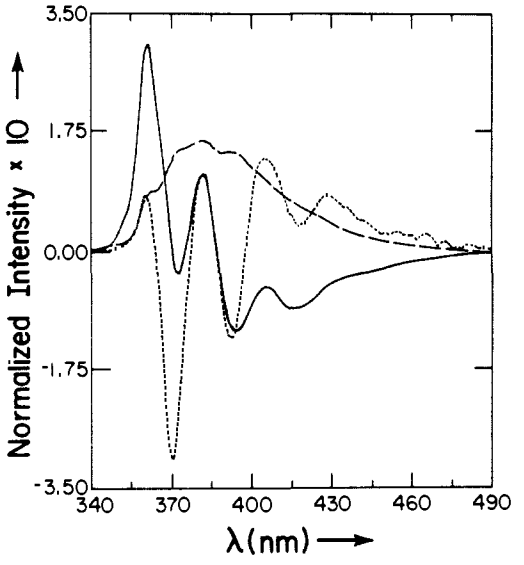

Figure 1. $\bar{V}_\alpha$ (— —), $\bar{V}_\beta$ (—), and $\bar{V}_\gamma$ (– – –) for the DNE/CCl_4 matrix. The four largest eigenvalues were 1.6113, 0.2650 × 10^{-1}, 0.1804 × 10^{-2}, and 0.1453 × 10^{-3}.

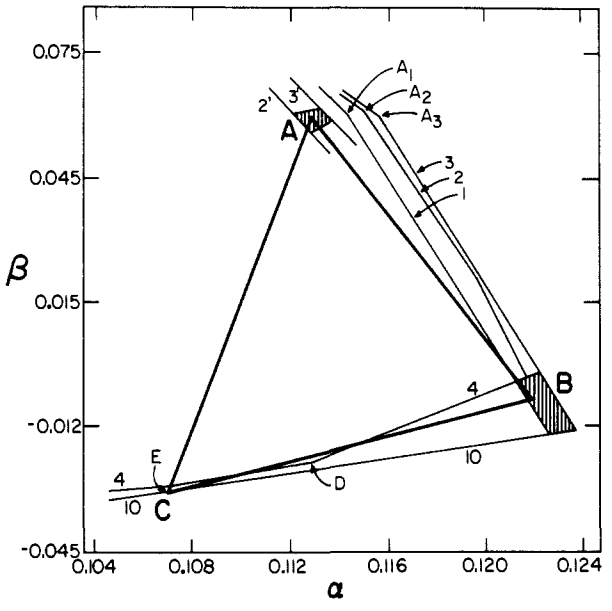

Figure 2. Projection of the coefficient triangle for the DNE/CCl_4 matrix on the α,β plane. Numbers next to lines give the number of negligibly small negative intensities in the appropriate region of the calculated spectra. Primed numbers give the number of small *positive* intensities in calculated spectra. K_{sv}'s and standard deviations as the selection of DNE-A coefficients is changed from A to A_1 to A_2 and to A_3 are as follows: $(K_{sv})_B$ = 8.5 ± 0.4, 8.0 ± 0.8, 7.8 ± 0.9, 7.5 ± 1.1 M^{-1}; $(K_{sv})_C$ = 4.9 ± 0.8, 5.2 ± 1.0, 5.3 ± 1.1, 5.4 ± 1.1 M^{-1}, respectively.

of the spectra, respectively, for negligibly small negative intensities. The numbers next to each line in Figure 2 give the number of such intensities in the corresponding spectral regions. As expected, small negative intensities were only found in the W_1 and W_2 regions designated in Figure 3. Definition of side BC proved the more difficult task. For instance, the line for four negative intensities shows an apparent turning point in region D, well removed from the expected point C that corresponds to coefficients for the independently obtained pure DNE-C spectrum. We suspect that the curvature at D is caused by experimental noise in the W_1 region of the spectra. Examination of the spectra corresponding to each point on the 4 negative intensity line shows that points on the lower portion of the line $0.113 \geq \alpha \geq 0.106$ give spectra with negative intensities in both W_{1a} and W_{1b} regions (Figure 3). Since, in principle, negative intensities in W_{1b} could correspond to negative contributions of spectrum DNE-B, one might be led to believe

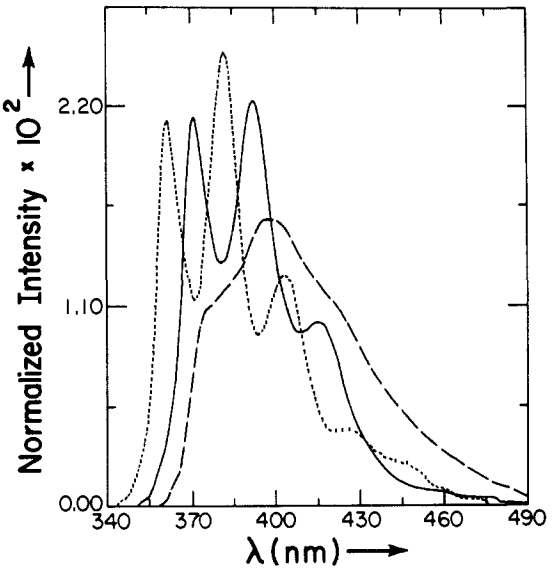

Figure 3. Pure component spectra for the DNE/CCl_4 system corrected for nonlinearity of instrumental response: DNE-A (– – –), DNE-B (—), DNE-C (— —); W_{1a} (343–350 nm), W_{1b} (350–357 nm), W_2 (475–490 nm).

that the limiting coefficients for DNE-C should be close to region D. In practice, however, noise at the onset region of the spectra is reflected in noise in the eigenvectors in the same region. Since, as the true coefficients for pure component spectrum DNE-C are approached, the combination of the three eigenvectors should simultaneously vanish in the 340–355-nm interval, the appearance of several small negative intensities in W_{1b} could be dominated by noise, rather than reflect the subtraction of spectrum DNE-B from spectrum DNE-C. Furthermore, examination of spectra for coefficients close to D indicate that the negative intensities in these spectra are caused by a negative contribution from the spectrum of component DNE-A, in violation of the basic assumption of the SM method. We conclude that D represents a false turning point and are secure in this conclusion since pure spectrum C was known from the treatment of the 366-nm data and its coefficients are at point C. It is gratifying that a very stable solution exists at point E (note the near touching of the 4 negative intensity line with the 10 negative intensity line) which is almost coincident with point C. We therefore chose point C as one corner of the triangle but could have chosen point E without significantly affecting the results of the PCA-SM treatment.

Acceptable trial coefficients for the spectrum of component DNE-B are expected to fall in the shaded region at the lower portion of the triangle. In the absence of additional information a point in the center of this region would give a very good estimation of spectrum B. The point B actually chosen corresponds to the coefficients for the independently obtained spectrum of DNE-B (see above) and is, as expected, within the region defined by our method.

The fact that point B fell on the line corresponding to one negative intensity in W_2 influenced our selection of point A_1 at the turning point of that line as the initial choice of coefficients for DNE-A. The accurate choice of A is hampered because it is based on intensities at the tail region of the spectra where phototube sensitivity is lowest and experimental noise contribution is largest. Stern–Volmer constants for components B and C based on point A_1 were largely independent of λ_{exc} (K_{sv}'s for component A are independent of the choice of point A). It seemed prudent, therefore, to utilize the independence of $(K_{sv})_B$'s and $(K_{sv})_C$'s on λ_{exc} as an additional constraint in refining the selection of point A.[12] Since agreement between the K_{sv}'s for the five λ_{exc} worsened when turning points on the lines with two and three zero intensities were used instead of A_1 it became necessary to consider the possibility that even point A_1 lies outside the desired triangle. To narrow down possible values for A, combination coefficients were determined for which the resultant spectra have very small *positive*

Table I. Fractional Contributions and CCl_4 Stern–Volmer Constants for DNE Conformers[a]

λ_{exc}, nm	x_a	x_b	x_c	K_{sv},[b] M^{-1} A	B	C
318	0.446 (1)	0.224 (1)	0.330 (1)	11.5 (13)	8.7 (3)	6.0 (5)
329	0.468 (3)	0.220 (4)	0.312 (5)	10.7 (2)	8.1 (2)	5.6 (8)
343	0.369 (1)	0.254 (4)	0.377 (4)	10.7 (5)	8.0 (3)	5.2 (8)
355	0.231 (1)	0.365 (5)	0.404 (7)	10.7 (5)	8.9 (4)	3.9 (6)
366	0.000	0.393 (3)	0.607 (3)		9.3 (10)	3.8 (4)
				10.8 (2)	8.5 (3)	4.9 (6)

[a] x_i's in MCH, 30 °C, no quencher; values in parentheses are uncertainties in last significant figure(s). [b] Data for λ_{exc} combined give K_{sv} values at bottom; note that 11.5 (13) means 11.5 ± 1.3.

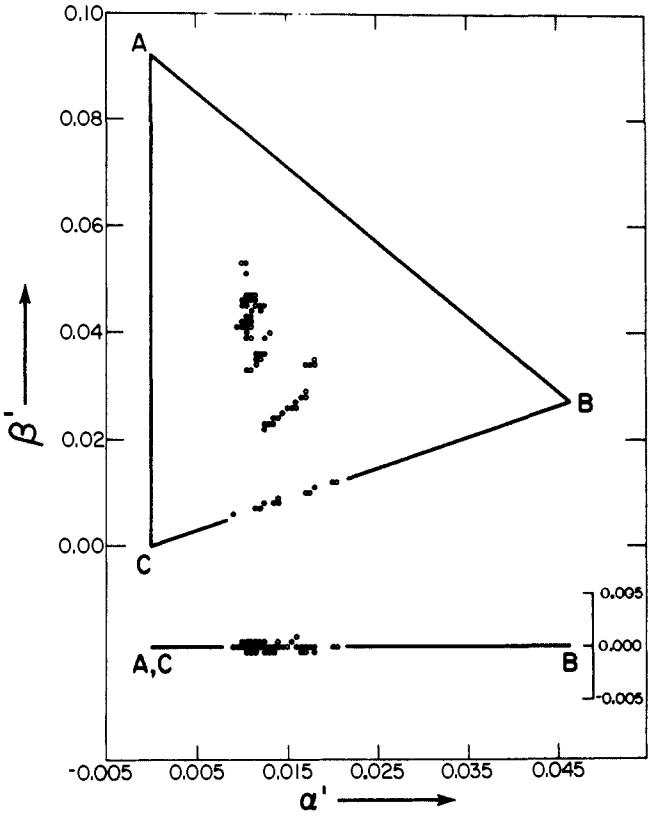

Figure 4. Orthogonal and edge views of triangle from plot of coefficients for DNE/CCl_4 systems; most points represent several independent experimental spectra.

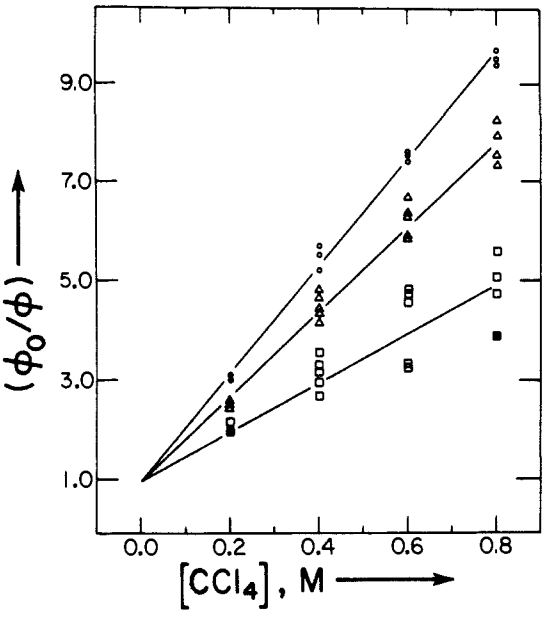

Figure 5. Stern–Volmer plots for CCl_4 quenching of resolved DNE conformer fluorescence: DNE-A (○), DNE-B (△), DNE-C (□). Solid figures represent multiple data points.

intensities (5×10^{-5}) in the W_2 region. This gave rise to lines 2′ and 3′ in Figure 2 which correspond to two and three such intensities, respectively. The shaded area in Figure 2 surrounding point A corresponds to the region in α,β,γ space leading to optimum agreement for the K_{sv}'s of component *B*. Point A was arbitrarily chosen at the center of that region. Orthogonal and edge views of the final triangle are shown in Figure 4, and fluorescence spectra corresponding to the selected pure component coefficients are shown in Figure 3. The spectra are corrected for nonlinearity in instrumental response. Fractional contributions for each component are given in Table I at each λ_{exc} at zero quencher concentration. Also given in Table I are Stern–Volmer constants for CCl_4 fluorescence quenching obtained at each λ_{exc} for each conformer. It can be seen that, within experimental uncertainty, the K_{sv} values are independent of λ_{exc}. Stern–Volmer plots for all the data combined are shown in Figure 5.

DNE Fluorescence Spectra at Several λ_{exc}, $[O_2]$. A set of DNE fluorescence spectra in MCH was obtained by using four O_2 concentrations and exciting at 257, 274, 294, 318, 329, 343, 355, and 367 nm. The set combined measurements from two independent experiments for which all spectra were recorded in triplicate. Saturation with O_2 and elimination of O_2 were achieved by bubbling with O_2 and Ar through the solutions, respectively.[17] An intermediate O_2 concentration was obtained by partial outgassing with O_2; its value, 5.3×10^{-3} M, was estimated by averaging intrapolated values from effective SV plots at each λ_{exc}. The final input matrix (136 × 150) consisted of 126 fluorescence spectra (340–489 nm) and five entries each of the pure DNE-B and DNE-C spectra obtained from the resolution of the data set with λ_{exc} = 367 nm (see above). Pure DNE-B and DNE-C spectra were substituted for scattered light-corrected 367-nm spectra because accurate definition of the BC side of the triangle was hindered by the narrow range of DNE-B/DNE-C ratios in the experimental spectra.[15] Examination of eigenvectors (Figure 6) and eigenvalues from the PCA treatment showed that this matrix too was comprised of three components. The results of the search for the triangle using the eigenvectors in Figure 6 are shown in Figure 7. The shaded region in the vicinity of point B is defined by the intersection of possible AB sides (1–3 negative intensities at the tail) and possible BC sides (1–11 negative intensities at the onset). Lines for 3–11 negative intensities at the onset of calculated spectra are nearly coincident at point C. The points B and C selected, though based on the coefficients of the pure component spectra included in the matrix, fall nicely in the predicted regions. The subtle turning point A_1 on the first negative intensity line (tail) is a potential choice for corner A of the triangle. Since the values of $(K_{sv})_B$ and $(K_{sv})_C$ (with $(K_{sv})_B$ somewhat larger than $(K_{sv})_C$) are available from the resolution of the 367-nm matrix and for that wavelength are independent of the choice of A, it seemed prudent to once again employ the behavior of the K_{sv}'s in refining the selection of A. Use of A_1 gave $(K_{sv})_B < (K_{sv})_C$ for the other λ_{exc}. Improved agreement between the K_{sv}'s was obtained by using the same procedure as in the CCl_4 case. The shaded region between lines for 1 and 3 slightly positive intensities at the tail of the spectra gave optimum K_{sv} behavior, and the center of this region was selected as point A. Orthogonal and edge views of the final triangle and the coefficients of the experimental spectra

Table II. Fractional Contributions and O_2 Stern–Volmer Constants for DNE Conformers[a]

λ_{exc}, nm	x_a	x_b	x_c	K_{sv},[b] M^{-1} A	B	C
257	0.327 (16)	0.249 (23)	0.424 (44)	158.7 (74)	63.2 (61)	59.2 (16.5)
274	0.293 (1)	0.304 (12)	0.403 (12)	157.4 (132)	56.1 (24)	61.0 (125)
294	0.299 (6)	0.372 (14)	0.329 (11)	156.4 (19)	53.2 (137)	64.5 (42)
318	0.454 (2)	0.235 (9)	0.311 (10)	162.6 (64)	60.9 (93)	76.2 (61)
329	0.473 (4)	0.232 (5)	0.294 (7)	176.5 (147)	77.8 (39)	62.2 (262)
343	0.387 (4)	0.274 (6)	0.339 (5)	166.7 (39)	69.5 (120)	68.8 (77)
355	0.241 (4)	0.329 (8)	0.430 (12)	172.9 (92)	75.7 (130)	70.9 (37)
366	0.004 (0)	0.405 (2)	0.591 (20)		64.6 (55)	63.8 (95)
367	0.006 (3)	0.375 (6)	0.620 (7)			
				164.5 (44)	65.2 (44)	65.7 (40)

[a] x_i's in MCH, 30 °C, no quencher; values in parentheses are uncertainties in last significant figure(s). [b] Data for λ_{exc} combined give K_{sv} values at bottom; note that 158.7 (74) means 158.7 ± 7.4.

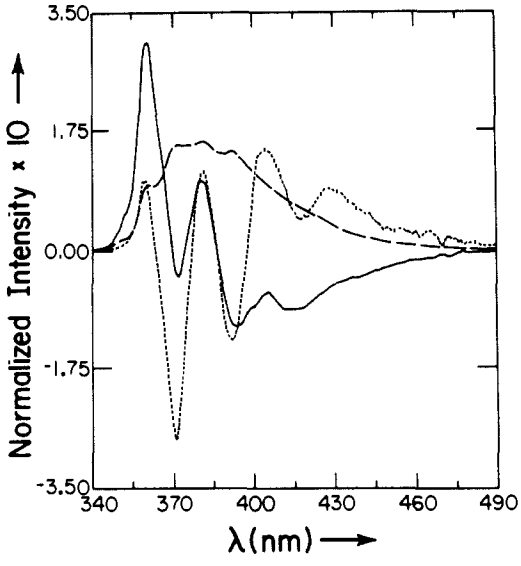

Figure 6. As in Figure 1, but for the DNE/O_2 matrix; the four largest eigenvalues were as follows: 0.9379, 0.1101 × 10^{-1}, 0.6111 × 10^{-2}, and 0.7593 × 10^{-4}.

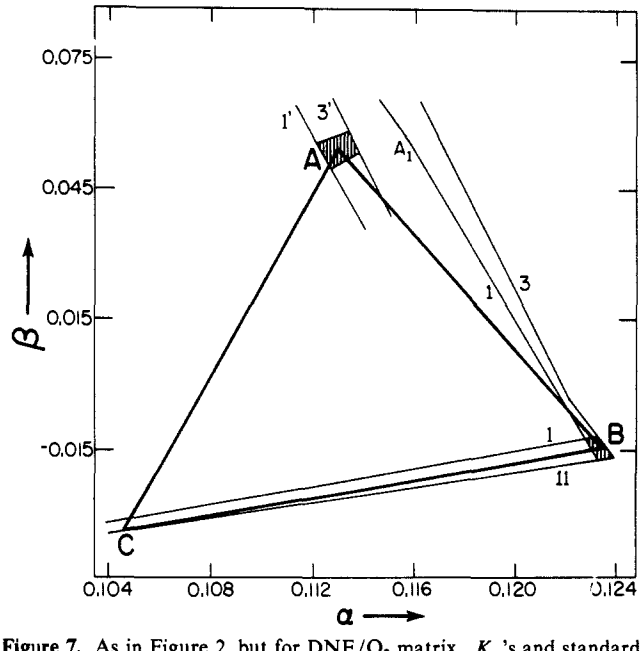

Figure 7. As in Figure 2, but for DNE/O_2 matrix. K_{sv}'s and standard deviations as the selection of DNE-A coefficients is changed from A to A_1 are as follows: $(K_{sv})_B$ = 65.1 ± 6.9, 50.9 ± 8.2 M^{-1}; $(K_{sv})_C$ = 65.8 ± 4.6, 69.7 ± 4.4 M^{-1}.

are shown in Figure 8. The resulting (corrected for nonlinearity of instrumental response), pure component spectra are shown in

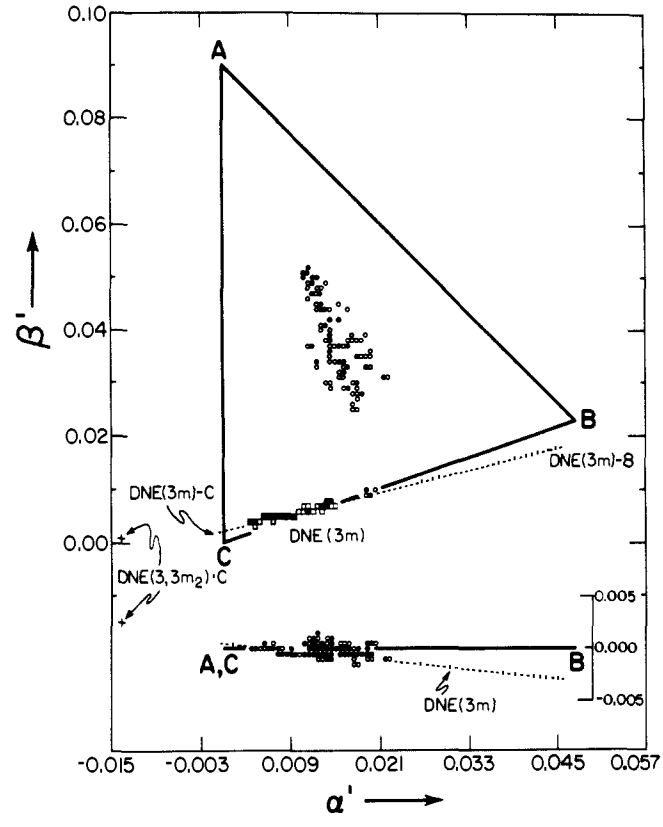

Figure 8. As in Figure 4, but for DNE/O_2 matrix; squares are coefficients for DNE(3m) spectra, + is for DNE(3,3′m_2).

Figure 9. Fractional contributions for each component are given in Table II for each λ_{exc} at zero quencher concentration. Also given in Table II are K_{sv} values for O_2 fluorescence quenching obtained at each λ_{exc} for each conformer. Stern–Volmer plots for all the data combined are shown in Figure 10.

DNE(3m) Fluorescence Spectra at Several λ_{exc}, [O_2]. A set of DNE(3m) fluorescence spectra in MCH was obtained by using argon, air, and O_2 saturated solutions and exciting at 255, 270, 290, 297, 316, 330, 344, and 367 nm. All spectra were recorded in triplicate. The input matrix for PCA-SM treatment consisted of 72 spectra with intensities recorded at each 1-nm interval in the 350–489-nm range. Resulting significant eigenvectors for the two-component solution are shown in Figure 11. Coefficients for experimental spectra adhere closely to the normalization line (Figure 12), and pure component limiting coefficients are readily found by monitoring for negligibly small negative intensities at the tail (DNE(3m)-B) and at the onset (DNE(3m)-C) of the spectra. Pure-component spectra are shown in Figure 13, and though strongly overlapping, clearly exhibit W_1 and W_2 regions required for a unique solution. Table III lists fractional contributions for each component at zero quencher concentration and

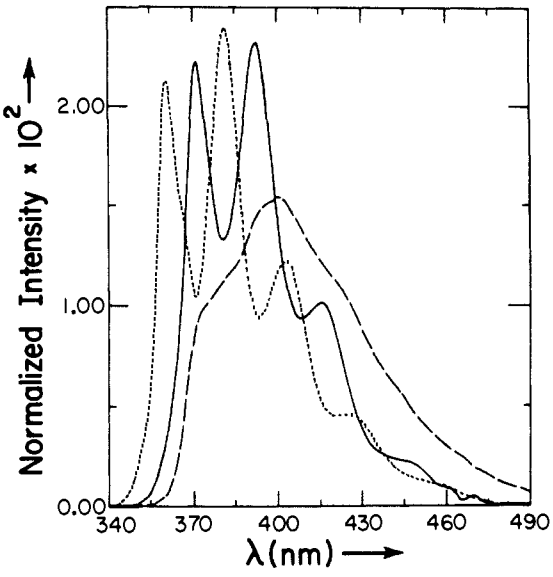

Figure 9. As in Figure 3, but for DNE/O_2 matrix.

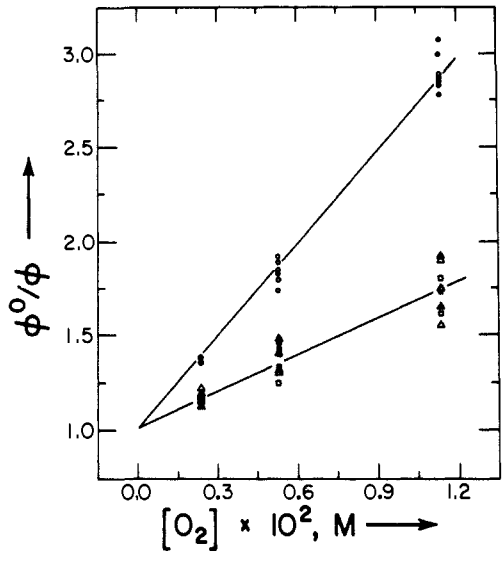

Figure 10. Stern–Volmer plots for O_2 quenching of resolved DNE conformer fluorescence: DNE-A (○), DNE-B (△), DNE-C (□).

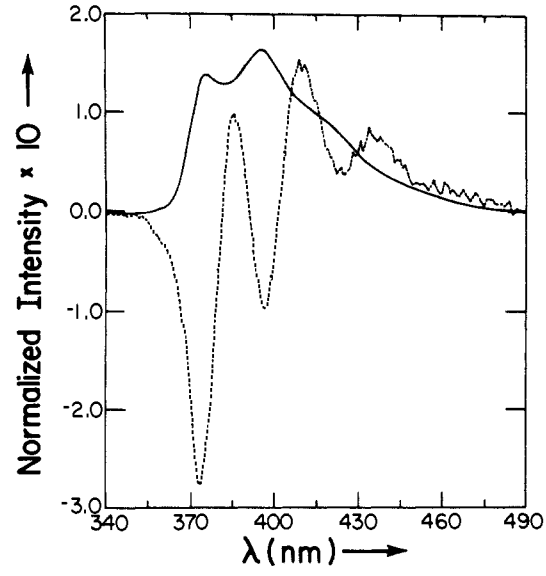

Figure 11. $\bar{V}_\alpha$ (—) and $\bar{V}_\beta$ (— —) for the DNE(3m)/O_2 matrix; the four largest eigenvalues were 0.9046, 0.9471 × 10^{-3}, 0.3361 × 10^{-4} and 0.1521 × 10^{-4}.

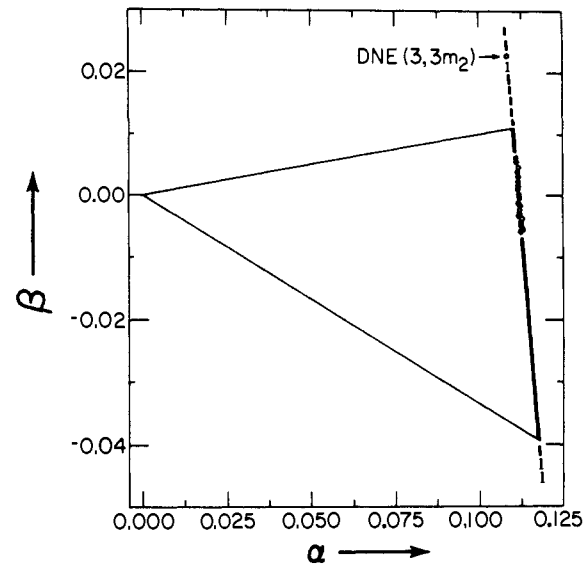

Figure 12. α,β plot for DNE(3m)/O_2 matrix; the normalization line of the vectors in Figure 11 is drawn through the points.

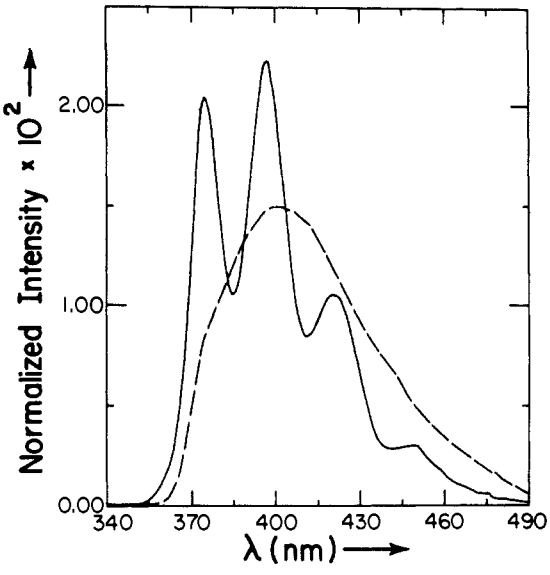

Figure 13. Pure component spectra for the DNE(3m) system corrected for nonlinearity of instrumental response: DNE(3m)-B (—), DNE-(3m)-C (— —).

Table III. Fractional Contributions and O_2 Stern–Volmer Constants for DNE(3m) Conformers[a]

λ_{exc}, nm	x_b	x_c	K_{sv},[b] M^{-1} B	C
255	0.176 (3)	0.825 (3)	94.8 (32)	65.7 (32)
270	0.144 (3)	0.856 (3)	94.1 (88)	60.9 (42)
290	0.287 (4)	0.713 (4)	88.8 (70)	60.3 (39)
297	0.306 (2)	0.694 (2)	92.2 (109)	57.9 (91)
316	0.248 (3)	0.752 (3)	95.5 (97)	66.7 (44)
330	0.207 (2)	0.793 (2)	92.1 (60)	64.7 (27)
344	0.182 (1)	0.818 (1)	92.6 (36)	60.3 (33)
			92.9 (27)	62.4 (18)

[a] x_i's in MCH, 30 °C, no quencher; values in parentheses are uncertainties in last significant figure(s). [b] Data for λ_{exc} combined give K_{sv} values at bottom; note that 94.8 (32) means 94.8 ± 3.2.

K_{sv} values as a function of λ_{exc}. Stern–Volmer plots for all the data combined are shown in Figure 14.

DNE(3,3′m_2) Fluorescence Spectra at Several λ_{exc}, [O_2]. A set of DNE(3,3′m_2) fluorescence spectra in MCH was obtained by using argon, air, and O_2 saturated solutions and exciting at 270, 290, and 330 nm. Since no change in the spectrum (Figure 15)

Table IV. Spectral Features in the Fluorescence of DNE Conformers[a]

band	λ_{max},[b] nm					
	DNE-A	DNE-B	DNE(3m)-B	DNE-C	DNE(3m)-C	DNE(3,3'm_2)-C
0–0	361 (362)	371 (371)	374	382_{sh} (381_{sh})	380_{sh}	393
0–1	382 (382)	392 (393)	397	401 (401)	401	415
0–2	404 (403)	415 (414)	419	421_{sh} (419_{sh})		439
0–3	423_{sh} (425_{sh})	449_{sh} (448_{sh})	≃450			

[a] Estimated uncertainties: ±1 nm for resolved maxima; ±5 nm for shoulders (sh). [b] For DNE, values in parentheses are from Figure 3 and the rest from Figure 9.

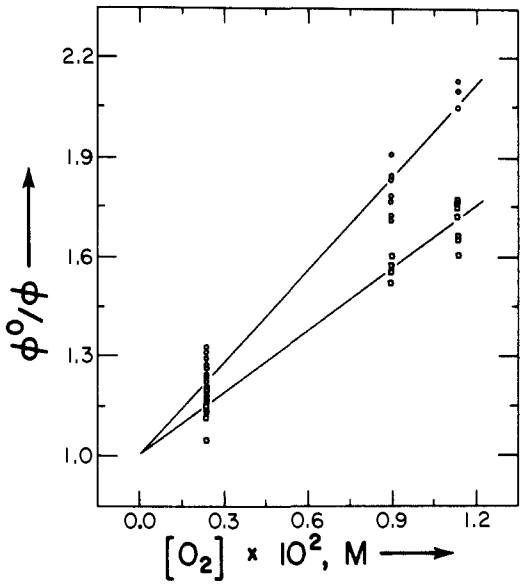

Figure 14. Stern–Volmer plots for O_2 quenching of resolved DNE(3m) conformer fluorescence: DNE(3m)-B (○), DNE(3m)-C (□).

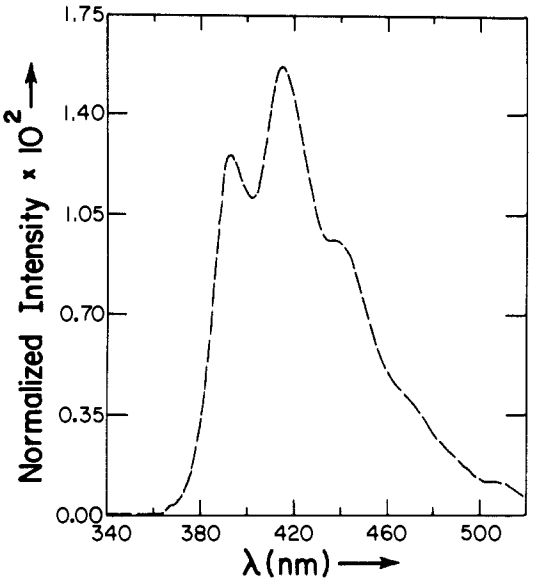

Figure 15. Fluorescence spectrum for DNE(3,3'm_2)-C corrected for nonlinearity of instrumental response.

could be discerned, the system was assumed to consist of a single component, DNE(3,3'm_2)-C. The Stern–Volmer plot for O_2 quenching of the fluorescence was insensitive to changes in λ_{exc} (Figure 16), giving K_{sv} = 42.1 ± 0.9 M^{-1}.

Absorption Spectra. Absorption spectra of DNE, DNE(3m), and DNE(3,3'm_2) in MCH at 30 °C are shown in Figure 17.

Discussion

X-ray crystallographic measurements show that the molecular structure of DNE in the crystal corresponds to DNE-A.[18] As is generally the case for naphthalenes, the C_1–C_2 bond (1.381 Å) in DNE-A is shorter than the C_2–C_3 bond (1.427 Å).[19b] Accordingly, DNE-A is expected to be the most planar of the three conformers having the shortest H–H distance, H_3–$H_{\alpha'}$ = 2.16 Å, in the completely planar geometry which can be relieved by a slight torsion of ca. 8° about the aryl–vinyl bonds.[19b] As the naphthyl groups assume the less extended arrangements in DNE-B and DNE-C, larger torsions are required to relieve H–H nonbonded interactions in the planar geometries.[19]

The conclusion that the fluorescence spectra of DNE conformers are progressively red-shifted with respect to each other was based initially on fluorescence spectra of DNE obtained at 4 K in crystalline *n*-pentane or *n*-hexane (Shpolskii matrices).[19] It was reasoned that the near-planarity of DNE-A favored its incorporation in the Shpolskii matrices where it gave rise to a quasi-line fluorescence spectrum, whereas DNE-B and/or DNE-C, being nonplanar, gave rise to an underlying red-shifted diffuse spectrum.[19] Our initial approximate resolution of DNE fluorescence spectra, based on the spectra of the conformationally restricted methyl derivatives, DNE(3m) and DNE(3,3'm_2), placed these

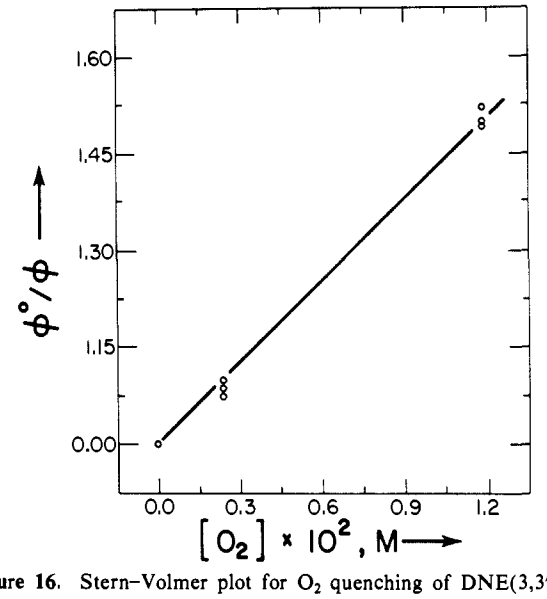

Figure 16. Stern–Volmer plot for O_2 quenching of DNE(3,3'm_2)-C fluorescence.

structural assignments to the fluorescence spectra on firm footing.[15] The present work has yielded two strikingly similar sets of DNE pure component spectra (Figures 3 and 9), which can independently be compared with the spectra of the methyl derivatives (Figures 13 and 15). Vibronic band features of these spectra are summarized in Table IV. Except for small red shifts due to methyl substitution (3–5 nm for monomethyl and 10–13 nm for dimethyl) the correspondence of these spectra is obvious. Also very clear is the progressive broadening of the vibronic features of the spectra as the nonplanarity of the conformers increases. The resolved DNE-A and DNE-B fluorescence spectra (Figures 3 and 9) are in excellent agreement with low-temperature spectra assigned to these conformers under a variety of conditions.[6b,13,14,19]

(17) IUPAC Analytical Chemistry Division, Commission on Solubility Data. "Oxygen and Ozone". In *Solubility Data Series*; Battino, R., Ed.; Pergamon: Oxford, 1981; Vol. 7.
(18) Shakked, Z., unpublished results quoted in ref 6b and ref 19.
(19) (a) Muszkat, K. A.; Wismontski-Knittel, T. *Chem. Phys. Lett.* **1981**, *83*, 87. (b) Muszkat, K. A.; Wismontski-Knittel, T. *J. Phys. Chem.* **1981**, *85*, 3427.

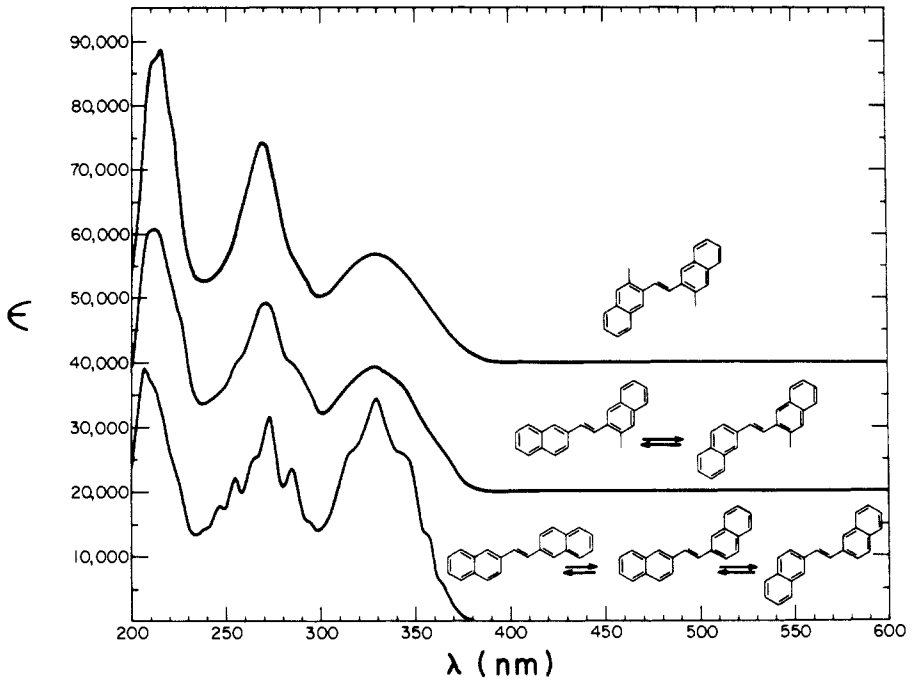

Figure 17. Absorption spectra of DNE, DNE(3m), and DNE(3,3'm_2) in MCH at 30 °C.

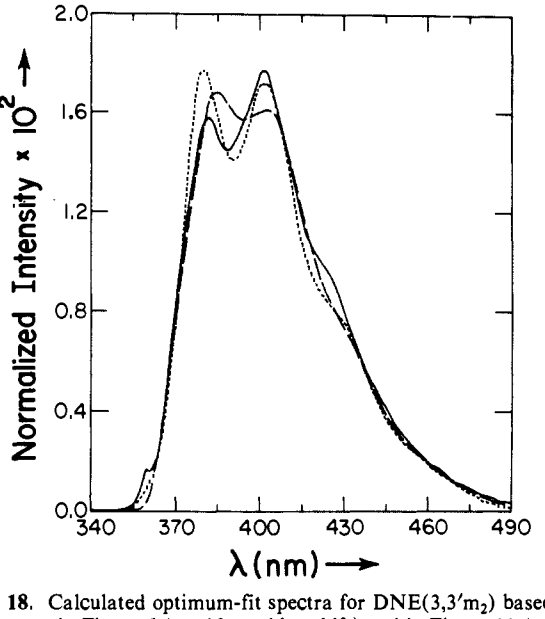

Figure 18. Calculated optimum-fit spectra for DNE(3,3'm_2) based on eigenvectors in Figure 6 (—, 12-nm blue shift) and in Figure 11 (— —, 9-nm blue shift); compare with experimental DNE(3,3'm_2) spectrum (– – –, 12-nm blue shift); spectra are uncorrected for nonlinearity of instrumental response.

Peak positions are also in very good agreement with those estimated from solution spectra obtained at room temperature by selective excitation.[6d] Comparison of our spectrum of DNE-C with those assigned to it at low temperatures is less straightforward due to the absence of a clearly resolved vibrational progression in fluid MCH solution at 30 °C. Bands at approximately 383, 407, and 433 nm which appear to be associated with this conformer have been obtained in polyethylene film (λ_{exc} = 380 nm, −100 °C),[6b] in crystalline *n*-hexane (λ_{exc} = 313 nm, 4 K),[19] and in ethanol (λ_{exc} = 362 nm, −175 °C).[14] Considerable deviations from planarity in this conformer at ambient temperatures could cause the loss of vibrational structure as indicated by our resolved DNE-C spectrum (Figures 3 and 9) and those of the corresponding methyl derivative spectra (Figures 13 and 15). The subtle sharpening of the DNE(3,3'm_2)-C spectrum was not expected. It suggests that the methyl groups constrain this conformer to somewhat more planar geometries.

A quantitative evaluation of the direct use of the methyl derivative fluorescence spectra as guides for the selection of pure component combination coefficients for the three conformers of unsubstituted DNE is now possible. DNE(3m) experimental spectra and the pure component spectra in Figure 13 were slightly blue-shifted (3 nm gave optimum results) and least-squares-fitted by using the eigenvectors in Figure 6. Very good fits were obtained, and the resulting DNE(3m) combination coefficients are plotted in Figure 8. The normal view of the triangle shows that coefficients for the experimental spectra fall close to the BC side and that those for DNE(3m)-B and DNE(3m)-C are remarkably close to corners B and C of the DNE triangle. A small systematic tilt of the DNE(3m) points with respect to the DNE normalization plane is revealed relative to the edge view of the plane. The shift of the DNE(3m) combination coefficients toward component C probably reflects the elimination of the factor of 2 statistical preference for component B in DNE as was inferred earlier.[15] The possibility that loss of structure in the fluorescence spectra of the C conformers of DNE and DNE(3m) reflects incorrect choices of combination coefficients was tested by least-squares fitting the appropriately blue-shifted (12 and 9 nm, respectively) spectrum of DNE(3,3'm_2) with the eigenvectors in Figures 6 and 11. In each case the optimum-fit spectrum reconstructed based on the eigenvectors was less structured than the original experimental DNE(3,3'm_2) spectrum (Figure 18). It follows that both the DNE and the DNE(3m) matrices fail to accept the DNE(3,3'm_2) spectrum as an exact solution for conformer C. Nonetheless, points corresponding to these fits fall close to point C and the DNE normalization plane in Figure 8 and to the normalization line in Figure 12. We conclude that when the method described in this paper fails to generate a satisfactory solution, the methyl derivative approach can provide a viable alternative for obtaining reasonable approximations of pure-component coefficients.

Since fluorescence quenching by O_2 is usually close to diffusion-controlled, the K_{sv} values in Table II should reflect mainly the difference in lifetime between the three conformers.[20] They indicate, therefore, that of the three conformers, DNE-A has the longest singlet lifetime, while DNE-B and DNE-C have nearly identical shorter lifetimes. This conclusion is consistent with results from pulsed excitation studies.[7a,13] Double exponential fluorescence decay has been reported for DNE solutions at room temperature in argon-flushed MCH (τ_1 = 2.1–2.3 nm, τ_2 = 7.2–7.5 ns)[7a] and

(20) Saltiel, J.; Atwater, B. W. *Adv. Photochem.* **1988**, *14*, 1.

in degassed cyclohexane, CH (τ_1 = 1.92 ± 0.04 nm, τ_2 = 8.6 ± 0.7 ns),[13] for several excitation wavelengths. Time-resolved emission spectra in MCH, λ_{exc} = 297 nm, yielded a relatively well-resolved spectrum for the long-lived species with λ_{max} at roughly 359, 381, 399, and 425 nm (30 ns delay time, 3 ns gate) and a broader spectrum for the short-lived species with new λ_{max} at approximately 371, 391, 415 (sh), and 450 (sh) nm (0 ns delay time, 3 ns gate).[13a] The spectrum of the long-lived species is in excellent agreement with our spectra for DNE-A, whereas the early spectrum shows mainly the spectral features of DNE-B and a small contribution from DNE-A and possibly from DNE-C (see Figures 3 and 9 and Table IV). Using τ_a = 7.35 ns and $\tau_b = \tau_c$ = 2.2 ns in MCH[7a] and neglecting small temperature effects gives $k_{qa}^{ox} = 2.24 \times 10^{10}$ M^{-1} s^{-1} and $k_{qb}^{ox} = k_{qc}^{ox} = 3.0 \times 10^{10}$ M^{-1} s^{-1} which, though not identical, are close to values expected for diffusion-controlled quenching rate constants involving oxygen.[20] It should be noted that the short-lived component was observed exclusively when the decay was monitored following excitation in the tail of DNE absorption where only DNE-B and DNE-C are expected to absorb, τ = 2.1 ns (λ_{exc} = 369 nm), 1.7 ns (λ_{exc} = 373 nm).[7a] Similar fluorescence excitation spectra for conformers B and C and the failure of O_2 to differentially quench these conformers account for the approximate behavior of the DNE/O_2 fluorescence spectral matrix as a two-component system.[15] Short lifetimes for conformers B and C can also be inferred from the K_{sv} values for O_2 quenching for DNE(3m), Table III, and DNE(3,3′m_2) (Figure 16).

In contrast to O_2, CCl_4 quenches the fluorescence of DNE-B and DNE-C differentially.[13b] Using the K_{sv} values in Table I, the lifetimes in ref 7a give $k_{qa} = 1.74 \times 10^9$ M^{-1} s^{-1}, $k_{qb} = 3.9 \times 10^9$ M^{-1} s^{-1}, and $k_{qc} = 2.2 \times 10^9$ M^{-1} s^{-1} for CCl_4 quenching of DNE-A, DNE-B, and DNE-C, respectively. The nearly 2-fold higher quenching efficiency of DNE-B for CCl_4 accounts for the easier resolution of the DNE/CCl_4 fluorescence spectral matrix into pure components. The mechanism of quenching by CCl_4 (e.g., enhanced intersystem crossing) remains to be established.

The λ_{exc} dependence of conformer fractional contributions to DNE fluorescence spectra is given in Tables I and II. Generally, the agreement between corresponding values in the two tables is excellent. Small discrepancies are real, as can be seen by fitting experimental spectra from each matrix with the eigenvectors of the other matrix and are probably due to our inability to manually reproduce λ_{exc} values in independent experiments. An uncertainty of ±1 nm in λ_{exc} would account for the largest deviations as can be seen by comparing x_b and x_c values in Tables I and II for λ_{exc} = 366 and 367 nm.

For double exponential fluorescence decay

$$I(t) = I_0[\alpha_1 \exp(-t/\tau_1) + \alpha_2 \exp(-t/\tau_2)] \quad (6)$$

the relationship of the parameters in eq 6 to the relative contributions of species characterized by the two lifetimes is $(x_1/x_2) = \beta = \alpha_1\tau_1/\alpha_2\tau_2$,[7] provided that emission is monitored with equal sensitivity over the entire spectral region. Decay parameters for DNE have been reported by Haas, Fischer, and Fischer[7a] under a variety of emission detection conditions. Unfortunately, though wavelength ranges for which emission was monitored are given, neither the relative transparency of the filters employed to select each range nor the sensitivity of the light detection system is known as a function of λ_{em}. This hampers a quantitative comparison between our fractional contributions, Tables I and II, and those inferred from the fluorescence decay measurements. A rough comparison can be attempted by assuming δ function behavior for the light filters employed and constant detection sensitivity over the emission wavelength range. It can be shown that under these conditions

$$\beta_{calcd} = \frac{x_b F_b}{x_a F_a} + \frac{x_c F_c}{x_a F_a} \quad (7)$$

where x_i is the fractional contribution of component i for a specified λ_{exc}, Tables I and II, and F_i is the area of the portion of the normalized spectrum of component *i* which is monitored (Figures 3 and 9). The condition $F_a = F_b = F_c = 1$ is fulfilled when all contributing emission wavelengths are equally monitored (λ_{em} independent detection sensitivity), and, in this special case, eq 7 reduces to $\beta_{calcd} = (x_b + x_c)/x_a$. Experimental and calculated β values, β_{obsd} and β_{calcd}, respectively, are listed in Table V. Though excitation wavelengths in this and previous studies do not coincide, a rough comparison of β_{obsd} and β_{calcd} can be achieved by considering similar λ_{exc} values. Agreement appears to exist only between β_{calcd} at λ_{exc} = 318 nm and β_{obsd} at λ_{exc} = 320 nm, and then only when the emission is monitored between 400–440 nm. In all other instances, calculated values based on eq 7 are larger than observed values, compare, for example, β_{calcd} = 5.4 at λ_{exc} = 355 nm with β_{obsd} = 1.89 at λ_{exc} = 354 nm. The discrepancy may be due in part to a decrease in detector sensitivity at the higher emission wavelengths which would lead to an underestimation of x_b and, especially x_c, in the fluorescence decay measurements. That more serious experimental difficulties may exist is indicated by decay parameters in ref 7a which gave β_{obsd} = 1.32 for λ_{exc} = 320 nm and λ_{em} > 490 nm. Reference to Figures 3 and 9 shows that only conformer C would be weakly detectable at those emission wavelengths.

Table V. Ratios of Fractional Conformer Contributions in DNE Fluorescence

λ_{exc}, nm	$(x_b + x_c)/x_a$[a]	β_{obsd}[b]	β_{calcd}[c]	λ_{em}, nm
257	2.06		3.4	400–490
265		2.01[d]		400–490
274	2.41		4.0	>390
280		1.53		>390
294	2.34		3.75	>390
			1.25	320–380
300		1.08		>390
		0.45		320–380
318	1.20 (1.24)		1.4	380–420
			1.9	400–440
320		0.84		380–420
		1.89		400–440
329	1.11 (1.14)			
340		1.29		>390
343	1.58 (1.71)		2.8	>390
354		1.89		>390
355	3.15 (3.33)		5.4	>390
358		2.63		>390
360		4.19		>390

[a] From Table I; values in parentheses from Table II. [b] Unless otherwise noted $\alpha_1\tau_1/\alpha_2\tau_2$ from ref 7a using τ_1 = 2.2 and τ_2 = 7.35 ns. [c] From results in Tables I and II and applicable portions of normalized pure component specra using eq 7. [d] From ref 13a.

Experimental Section

Materials. **Methylcyclohexane** from Baker (Photrex) was used as received; reagent grade MCH from Baker or Aldrich was washed with concentrated sulfuric acid, stirred over several portions of fuming sulfuric acid, washed with water followed by aqueous sodium bicarbonate, dried over sodium sulfate, and distilled. In all instances the treated MCH matched or exceeded the UV transparency of the Baker (Photrex) MCH. **Carbon tetrachloride** from Mallinkrodt (SpectrAR) was distilled prior to use. ***trans*-1,2-Di(2-naphthyl)ethene.** A previously described method was followed,[21] involving a Perkin condensation of 2-naphthylacetic acid and 2-naphthaldehyde, decarboxylation of the intermediate acrylic acid, and iodine-catalyzed isomerization of the resulting cis–trans mixture of alkenes. The crude trans product was sublimed at 180 °C (0.005 Torr), and the sublimate was recrystallized from benzene to give colorless crystals of *trans*-1,2-di(2-naphthyl)ethene, mp 257.5–259.0 °C (lit.[21] mp 258–259 °C). **2-(Bromomethyl)-3-methylnaphthalene.** 2,3-Dimethylnaphthalene was treated with *N*-bromosuccinimide in refluxing carbon tetrachloride according to a previously described procedure.[22] The crude product was recrystallized twice from hexane to give a sample of 2-bromomethyl-3-methylnaphthalene that was shown by GC/MS analysis to be 90% pure, contaminated with 7% 2,3-bis(bromomethyl)naphthalene and 3% 2,3-dimethylnaphthalene; this sample, with mp 83–86 °C (lit.[23]

(21) Everett, J. L.; Kon, G. A. R. *J. Chem. Soc.* **1948**, 1601–1603.
(22) Lecocq, J. *Ann. Chim. (Paris)* **1948**, [*12*], *3*, 62.
(23) MacCorquodale, D. W.; Cheney, L. C.; Binkley, S. B.; Holcomb, W. F.; McKee, R. W.; Thayer, S. A.; Doisy, E. A. *J. Biol. Chem.* **1939**, *131*, 357–370.

mp 104-105 °C), was used without further purification. ***trans*-1-(3-Methyl-2-naphthyl)-2-(2-naphthyl)ethene.** A sample of 2-(bromomethyl)-3-methylnaphthalene was converted to the corresponding phosphonium salt by treatment with triphenylphosphine in refluxing xylene. This salt was subjected to a Wittig reaction with 2-naphthaldehyde, by using a previously described phase-transfer method employing 50% aqueous sodium hydroxide and dichloromethane.[24] The crude solid product was digested with a 70/30 mixture of ethanol and water to remove the soluble triphenylphosphine oxide. The residual insoluble material was shown by GC/MS analysis to consist of a mixture of the cis and trans isomers of the desired alkene. This material was isomerized to the trans isomer by dissolving it in toluene containing a trace amount of iodine and irradiating the resulting solution with visible light. After the isomerization was shown to be complete by GC analysis, the solution was washed in a separatory funnel with aqueous 5% sodium thiosulfate solution, and the organic layer was separated, dried over anhydrous sodium sulfate, filtered, and rotary evaporated. The solid residue recrystallized twice from toluene to give *trans*-1-(3-methyl-2-naphthyl)-2-(2-naphthyl)ethene, mp 162.1-162.4 °C: ^{1}H NMR (200.1 MHz, $CDCl_3$) δ 8.103, 7.910, and 7.648 (br s, 1 H each, H-1, H-1′, H-4), 7.883-7.626 (complex m, 6 H), 7.506-7.384 (complex m, 4 H), 7.563 and 7.318 (AB q, 2 H, H-α and H-α', J = 16.1 Hz), 2.625 (s, 3 H, methyl). Anal. Calcd for $C_{23}H_{18}$: C, 93.84; H, 6.16. Found: C, 93.73; H, 6.20. ***trans*-1,2-Di(3-methyl-2-naphthyl)ethene.** A sample of 3.10 g (35 mmol) of 2-nitropropane dissolved in 5 mL of dry methanol was mixed with a solution prepared from the reaction of 0.83 g (36 mmol) of sodium with 30 mL of dry methanol. This material was stirred magnetically at room temperature while a solution of 6.56 g (28 mmol) of 2-(bromomethyl)-3-methylnaphthalene in 300 mL of dry methanol was added dropwise over 45 min. After the reaction mixture had been stirred for an additional 20 h, it was diluted with 250 mL of dichloromethane and washed in a separatory funnel with 2 100-mL portions of aqueous 10% sodium hydroxide solution and 1 200-mL portion of water. The organic layer was separated, dried over anhydrous magnesium sulfate, filtered, and rotary evaporated. The solid residue was recrystallized from 100 mL of hexane to give 3.24 g (68%) of off-white 3-methyl-2-naphthaldehyde, mp 118.0-119.2 °C (lit.[25] mp 124-125 °C). With the phase transfer method and the workup procedure described in the preceding paragraph, this aldehyde was subjected to a Wittig reaction with the phosphonium salt derived from the reaction of triphenylphosphine with 2-(bromomethyl)-3-methylnaphthalene. The crude product was recrystallized twice from toluene and then sublimed at 200 °C (0.005 Torr) to give *trans*-1,2-di(3-methyl-2-naphthyl)ethene as a faintly yellow solid with mp 218-219 °C: ^{1}H NMR (200.1 MHz, $CDCl_3$) δ 8.081 (s, 1 H, H-1), 7.859 (X part of ABX, 1 H, H-5 or H-8, $J_o + J_m$ = 9.5 Hz), 7.757 (X part of ABX, 1 H, H-8 or H-5, $J_o + J_m$ = 9.5 Hz), 7.659 (s, 1 H, H-4), 7.454 (s, 1 H, H-α), 7.431 (two coincident AB parts of ABX patterns, 2 H, H-6 and H-7, $J_o + J_m$ = 9.5 Hz), 2.626 (s, 3 H, methyl); MS, m/z 308 (M^+), 293, 278. Anal. Calcd for $C_{24}H_{20}$: C, 93.46; H, 6.54. Found: C, 93.24; H, 6.57.

General Procedures. Melting points were measured with a Thomas-Hoover oil-bath apparatus and are uncorrected. Elemental analyses were performed by M-H-W Laboratories, Phoenix, AZ. ^{1}H NMR spectra were determined at 17 °C in deuteriochloroform solution with tetramethylsilane as an internal standard using an IBM WP-200 SY spectrometer operating at 200.1 MHz. GC/MS analyses were carried out with a Hewlett-Packard 5890 gas chromatograph interfaced with a Hewlett-Packard 5970 mass selective detector. Sublimations at reduced pressure were accomplished as described elsewhere.[26] UV absorption measurements were carried out with a Perkin-Elmer Lambda 5 spectrophotometer. Luminescence measurements were made with a Hitachi/Perkin-Elmer fluorescence spectrometer as previously described.[16] PCA-SM calculations were also carried out as previously described.[16] Spectral input matrices, described in the Results section, consisted of uncorrected fluorescence spectra. Pure component fluorescence spectra were corrected for instrumental response, and fractional contributions were based on corrected spectra. Correction factors for fluorescence intensity values were empirically obtained at 0.5-nm intervals by the method described by Parker[27] employing a General Electric (no. 7429/36) tungsten lamp operated at 35 amperes. The spectral output of this lamp at various wavelengths had previously been determined relative to a National Bureau of Standards standardized tungsten lamp manufactured by The Eppley Laboratory Inc. (EPT-1109). Light from the tungsten lamp was reflected off a block of magnesium carbonate through a lens into the emission monochromator of the fluorescence spectrometer.

Acknowledgment. Work at Florida State University was supported by NSF Grant CHE-8713093.

Registry No. *trans*-DNE, 2753-11-9.

Supplementary Material Available: Graphs of eigenvectors, pure component spectra, and coefficient triangle for the DNE/O_2, 367-nm matrix (3 pages). Ordering information is given on any current masthead page.

(24) Warner, J. C.; Anastas, P. T.; Anselme, J. *J. Chem. Educ.* **1985**, *62*, 346.
(25) Shields, J. E.; Bornstein, J. *Chemistry and Industry* **1967**, 1404-1405.
(26) Mallory, F. B. *J. Chem. Educ.* **1962**, *39*, 261.
(27) Parker, C. A. *Photoluminescence of Solutions*; Elsevier: Amsterdam, 1968; pp 252-258.

Many-Body Potential for Molecular Interactions

Allison E. Howard, U. Chandra Singh,† Martin Billeter,‡ and Peter A. Kollman*

Contribution from the Department of Pharmaceutical Chemistry, University of California—San Francisco, San Francisco, California 94143. *Received June 11, 1987*

Abstract: We have included both atomic polarizability and nonadditive exchange repulsion terms to a molecular mechanical force field and then utilized this force field to calculate complexation enthalpies for a series of crown ethers and ions. Using this model for both uncomplexed and complexed crown ethers, we have been able to calculate relative conformation energies and cation complexation enthalpies in which the relative and absolute agreement to experimental values are satisfactory. These results provide further evidence of the merit in including many-body terms in molecular mechanical calculations for which highly polarizable atoms or ionic interactions are treated. It is anticipated this implementation may be especially significant for macromolecular systems of biological interest.

Crown ethers have fascinated scientists of different disciplines for a multitude of reasons since their discovery by Pederson.[1] They are of interest to some scientists because they may be thought of as model systems for the study of binding interactions as found in molecule/drug or enzyme/substrate complexes.[2] This was the rationale that first motivated Wipff, Weiner, and Kollman[3] to study the conformational flexibility and the cation and binding specificity in the interaction of 18-crown-6 with alkali-metal cations

† Current address: Laboratory of Molecular Biology, Scripps Clinic and Research Foundation, La Jolla, CA 92037.
‡ Current address: Institut für Molekularbiologie und Biophysik, ETH-Hönggerberg, CH-8093 Zürich, Switzerland.

(1) Pederson, C. J. *J. Am. Chem. Soc.* **1967**, *89*, 7017.
(2) Kellogg, R. M. In *Host Guest Complex Chemistry/Macrocycles*; Vögtle, F., Weber, E., Eds.; Springer-Verlag: New York, 1985.
(3) Wipff, G.; Weiner, P.; Kollman, P. *J. Am. Chem. Soc.* **1982**, *104*, 3249.

0002-7863/88/1510-6984$01.50/0